AIAA JOURNAL
Vol. 32, No. 7, July 1994

Linear Disturbances in Hypersonic, Chemically Reacting Shock Layers

Greg Stuckert* and Helen L. Reed†
Arizona State University, Tempe, Arizona 85281

The effects of equilibrium- and nonequilibrium-air chemical reactions on the linear stability of a Mach 25, 10-deg half-angle sharp-cone shock layer are investigated. First, the basic state is computed using the parabolized Navier-Stokes equations with a shock-fitting scheme. This eliminates spurious numerical oscillations that could adversely affect the stability analysis. Spatial stability analyses are then described for three different approximations of the physics: perfect gas, air in local chemical equilibrium, and air in chemical nonequilibrium. It is shown in both the equilibrium- and nonequilibrium-air calculations that the second mode of Mack is shifted to lower frequencies. This is attributed to the increase in the size of the region of relative supersonic flow due to the lower speeds of sound in the relatively cooler boundary layers. Finally, in the equilibrium air calculations, modes that travel supersonically relative to the inviscid region of the shock layer are shown to exist. These modes are a superposition of incoming and outgoing disturbances whose magnitude oscillates with the distance normal to the wall in the inviscid region of the shock layer. This oscillatory behavior is possible only because the shock standoff distance is finite.

Nomenclature

a = speed of sound (nondimensionalized by V_∞^*)
c = phase speed of the disturbances (nondimensionalized by V_∞^*)
c_p = specific heat at constant pressure of the gas mixture per unit mass (nondimensionalized by $\mathcal{R}^*/\hat{M}_\infty^*$)
E_t = total energy of the mixture per unit volume (nondimensionalized by $\rho_\infty^* \mathcal{R}^* T_\infty^*$)
h = mixture enthalpy per unit mixture mass (nondimensionalized by $\mathcal{R}^* T_\infty^*/\hat{M}_\infty$)
$\hat{h}_i$ = enthalpy of species i per mole of species i (nondimensionalized by $\mathcal{R}^* T_\infty^*$)
h_3 = $(r + y \cos \varepsilon)^m$ (nondimensionalized by L_{ref}^m)
$\hat{J}_i$ = molar flux of species i (nondimensionalized by $\mu_\infty^*/L_{\text{ref}}\hat{M}_\infty^*$)
k = mixture thermal conductivity (nondimensionalized by $\mu_\infty^*(\mathcal{R}^*/\hat{M}_\infty^*)$
L_{ref} = reference length (dimensional)
M = Mach number (ratio of flow speed to sound speed)
$\hat{M}$ = molecular weight of the mixture (nondimensionalized by the freestream value)
$\hat{M}_k$ = molecular weight of species k (nondimensionalized by $\hat{M}_\infty^*$)
m = 0 for two-dimensional flow; 1 for axisymmetric flow
p = mixture pressure (nondimensionalized by $\rho_\infty^* \mathcal{R}^* T_\infty^*/\hat{M}_\infty^*$)
p_i = partial pressure of species i (nondimensionalized by $\rho_\infty^* \mathcal{R}^* T_\infty^*/\hat{M}_\infty^*$)
$\boldsymbol{q}$ = heat flux (nondimensionalized by $\mu_\infty^* \mathcal{R}^* T_\infty^*/L_{\text{ref}}\hat{M}_\infty^*$)
$\boldsymbol{Q}$ = $y_\eta \boldsymbol{U} = y_\eta h_3(\rho, \rho u, \rho v, \rho w, E_t, \rho\sigma_i)^T$
r = distance from the body axis to the surface (nondimension-alized by L_{ref}); see Fig. 1
Re_L = Reynolds number based on the length scale L_{ref}, $\rho_\infty^* V_\infty^* L_{\text{ref}}/\mu_\infty^*$
Re_x = Reynolds number based on the length scale x^*, $\rho_\infty^* V_\infty^* x^*/\mu_\infty^*$
R_i = molar rate of production of species i
$\mathcal{R}^*$ = universal gas constant, 8.3143 J/(gmole·K)
$s(\eta; a_s, b_s)$ = stretching function
$\boldsymbol{S}_{ij}$ = stress tensor (nondimensionalized by $\mu_\infty^* V_\infty^*/L_{\text{ref}}$)
T = mixture temperature (nondimensionalized by T_∞^*)
t = time (nondimensionalized by $L_{\text{ref}}/V_\infty^*$)
$\boldsymbol{U}$ = vector of conservative dependent (state) variables, $h_3(\rho, \rho u, \rho v, \rho w, E_t, \rho\sigma_i)^T$
u = mass-averaged tangential velocity component (nondimensionalized by V_∞^*)
V_∞^* = magnitude of freestream velocity vector
v = mass-averaged body-normal velocity component (nondimensionalized by V_∞^*)
w = spanwise (two-dimensional) or circumferential (axisymmetric) velocity component (nondimensionalized by V_∞^*)
x = arclength measured along a meridian (axisymmetric) or in the surface along a line perpendicular to the leading edge (two-dimensional) (nondimensionalized by L_{ref}); see Fig. 1
y = distance measured along the coordinate normal to the body surface (nondimensionalized by L_{ref}); see Fig. 1
y_c = distance of the critical point above the vehicle's surface (nondimensionalized by L_{ref})
y_1 = distance of the relative sonic point above the vehicle's surface (nondimensionalized by L_{ref})
z = spanwise distance (two-dimensional; nondimensionalized by L_{ref}) or angle measured circumferentially around the body axis (axisymmetric); see Fig. 1
α = (complex) wave number in streamwise direction, nondimensionalized with δ^* unless otherwise noted
$\alpha_{s(n)}$ = wave number of the nth inviscid neutral disturbance with phase speed equal to the tangential velocity component at the generalized inflection point
β = (real) wave number in the spanwise or circumferential direction
Δ = shock standoff distance (nondimensionalized by L_{ref})
δ^* = boundary-layer length scale, $x^*/\sqrt{Re_x}$
ε = angle between body surface and body axis; see Fig. 1
η = independent variable ranging along the coordinate line perpendicular to the body surface from 0 at the body to 1 at the bow shock

Received March 6, 1993; revision received Jan. 28, 1994; accepted for publication Jan. 31, 1994.

*Research Assistant, Department of Mechanical and Aerospace Engineering; currently Research Scientist, DynaFlow, Inc., P.O. Box 21-319, Columbus, OH 43221. Member AIAA.

†Director, Aerospace Research Center, and Professor, Department of Mechanical and Aerospace Engineering. Associate Fellow AIAA.

μ = mixture viscosity (nondimensionalized by the freestream value)
ρ = mixture mass density (nondimensionalized by the freestream value)
ρ_k = mass density of species "k" (nondimensionalized by ρ^*_∞)
σ_k = ratio of species "k" concentration to mixture mass density (nondimensionalized by $1/\hat{M}^*_\infty$)
ω = angular frequency of the disturbance state (nondimensionalized by V^*_∞/δ^* unless otherwise noted)
$\wedge$ = molar quantity
$-$ = based on velocity relative to that of mean flow

Subscripts (except where explicitly noted)

a = amplitude function
b = basic-state value
d = disturbance value
e = boundary-layer edge value
I = inviscid part
i = imaginary part of complex number
r = real part of complex number
s = evaluated at the generalized inflection point
V = viscous part
w = value at the wall (vehicle surface)
∞ = preshock (freestream) reference state

Superscripts (except where explicitly noted)

i = evaluated at ξ station i
T = transpose
$*$ = dimensional quantity

I. Introduction

THE resurgence of interest in hypersonic flight in the early 1980s has driven researchers to model high-enthalpy flows more accurately by accounting for chemical reactions in their computational fluid dynamics (CFD) simulations. These simulations are vital for design because of the difficulty of making detailed measurements in such severe, high-temperature environments.

To accurately simulate the flow, however, they must also model the transition of the flow from a laminar state to turbulence. This is very difficult to do given our lack of knowledge about transition in chemically reacting flows. Here we present some results of a theoretical/computational study of the linear, spatial growth of chemically reacting disturbances in a Mach 25 sharp-cone shock layer. The growth of these small disturbances, as for incompressible flows and supersonic flows, is thought to be the precursor of transition in the low-disturbance environment expected in flight.

Prior knowledge that we can draw on pertains to the high-Mach-number, low-enthalpy flows of perfect gases. Here, a number of researchers have contributed to our understanding.

Lees and Lin[1] studied the temporal growth of two-dimensional inviscid disturbances in parallel, perfect-gas flows. (Analogous results for three-dimensional disturbances in a three-dimensional boundary layer can be found using the "tilde" coordinate system described by Mack.[2] This coordinate system is rotated so that the "x" direction coincides with that of the phase velocity.) Lees and Lin classified the disturbances according to the disturbance phase speed relative to the boundary-layer edge velocity:

Subsonic:

$$u^*_{be} - c^*_r < a^*_{be} \tag{1a}$$

Sonic:

$$u^*_{be} - c^*_r = a^*_{be} \tag{1b}$$

Supersonic:

$$u^*_{be} - c^*_r > a^*_{be} \tag{1c}$$

One of their most important results was that a neutral subsonic solution will exist if and only if there is a generalized inflection point y^*_s in the boundary layer. A generalized inflection point is a point in the flow profile where

$$\frac{\partial}{\partial y^*}\left(\rho^*_b \frac{\partial u^*_b}{\partial y^*}\right) = 0 \tag{2}$$

The proof that the presence of a generalized inflection point implies the existence of a neutral solution requires that the local flow velocity be subsonic throughout the boundary layer relative to the disturbance phase speed. In this case, the phase speed c^*_s is equal to the tangential velocity component at the generalized inflection point y^*_s. Moreover, the neutral solution will have a unique wave number α^*_s.

Mack[2] has subsequently shown that if a region exists within the boundary layer where the local flow velocity is supersonic relative to the phase speed, then there is not one discrete wave number but an infinite set corresponding to c^*_s. He has demonstrated this numerically and also theoretically by describing the change in the character of the linear inviscid stability equations when the local flow Mach number relative to the phase speed becomes supersonic. Mack refers to these additional modes as the "higher subsonic neutral modes" (Ref. 1, pp. 11.11–11.16) or "inflectional neutral waves."[3]

The inflectional neutral solutions have phase speed $c^*_s > u^*_{be} - a^*_{be}$ because they are subsonic. At the same time, $c^*_s \le u^*_{be}$ because $c^*_s = u^*_b(y_s) \le u^*_{be}$. In addition to the inflectional solutions, Mack[2] has also found neutral subsonic solutions with phase speed c^*_r such that $u^*_{be} + a^*_{be} \ge c^*_r \ge u^*_{be}$. Although these additional neutral modes are still subsonic relative to the freestream, they are supersonic relative to the local flow velocity within some part of the boundary layer. Hence, these modes are also infinite in number. However, since there is no point where $u^*_b = c^*$ (a critical point in the inviscid theory) for this range of phase speeds, Mack[2] refers to them as regular neutral solutions or noninflectional neutral waves.

Other investigators have also independently studied the linear stability of compressible boundary layers. However, virtually all of them have focused on perfect-gas flows. Some exceptions are Malik,[4,5] Menon et al.,[6] and Grinstein and Kailasanath.[7] Malik investigated the stability of an equilibrium-air boundary layer on an adiabatic flat plate. Menon et al. studied the spatial inviscid instability of a two-dimensional free shear layer undergoing finite rate chemical reactions. They assumed an analytic form for the basic state and modeled the combustion of oxygen and hydrogen. They concluded that the finite rate reactions had a significant effect on the stability of the flow, destabilizing it while lowering the phase speeds of the disturbances. Grinstein and Kailasanath used direct numerical simulations to study the transitional flow of a two-dimensional mixing layer of a hydrogen-nitrogen stream and an oxygen-nitrogen stream that react to produce water vapor. Disturbances in the mixing layer were forced by a fluctuating cross-stream velocity component at the inflow boundary. Finally, some work involving the stability of chemically reacting flows has also been done in the former Soviet Union.

Here the stability of viscous disturbances in chemical nonequilibrium is analyzed and compared with 1) the stability of the flow assuming that it is in local chemical equilibrium and 2) the stability of the flow assuming that it is a perfect gas.

II. Governing Equations

The stability of a steady, hypersonic, laminar shock layer is governed by the unsteady Navier-Stokes equations for a chemically reacting gas. We use a five-component model for dissociated air: O_2, N_2, NO, N, and O. Only the effects of dissociation are included; those of ionization are not. It is also assumed that the time taken for the different internal energy modes of the mixture (such as translational, rotational, vibrational, and electronic) to reach a state of local (pointwise) equilibrium is much shorter than any characteristic chemical-reaction time or flow-traversal time. The gas state can then be approximated as one of local thermal equilibrium (sometimes this is not a good approximation; for instance, the vibrational energy may not be in equilibrium behind a strong bow shock created by a blunt body) and its internal energy can be de-

scribed by only a single temperature. [In other words, the gas composition is essentially frozen during the short time it takes for the modes of internal energy to reach equilibrium. However, depending on the rates of the reactions, the gas composition may change over a time characteristic of the flow (i.e., time taken to convect or diffuse a characteristic distance).] Finally, the mixture is assumed to be one of thermally perfect gases so that the specific heats are functions of temperature only and Dalton's law of partial pressures applies.

The coordinate system for both the basic-state and stability analysis fits the body and bow shock as coordinate lines and is obtained from the following transformation from body-intrinsic coordinates[8] (Fig. 1):

$$t = \tau \tag{3a}$$

$$x = \xi \tag{3b}$$

$$\zeta = z \tag{3c}$$

$$y = \Delta(\xi, \zeta, \tau) \cdot s(\xi, \eta, \zeta) \tag{3d}$$

This makes it easy to accurately enforce the boundary conditions. In terms of this shock-fitted coordinate system, the Navier-Stokes equations can be written[9–13] as follows:

$$\frac{\partial}{\partial\tau}(y_\eta \boldsymbol{U}) + \frac{\partial}{\partial\xi}(y_\eta \boldsymbol{E}) + \frac{\partial}{\partial\eta}(-y_\tau \boldsymbol{U} - y_\xi \boldsymbol{E} + \boldsymbol{F} - y_\zeta \boldsymbol{G}) + y_\eta \boldsymbol{H} - y_\eta \boldsymbol{R} = 0 \tag{4}$$

where

$$\boldsymbol{E} = \boldsymbol{E}_I - \boldsymbol{E}_V \tag{5a}$$

$$\boldsymbol{F} = \boldsymbol{F}_I - \boldsymbol{F}_V \tag{5b}$$

$$\boldsymbol{G} = \boldsymbol{G}_I - \boldsymbol{G}_V \tag{5c}$$

$$\boldsymbol{H} = \boldsymbol{H}_I - \boldsymbol{H}_V \tag{5d}$$

$$\boldsymbol{U} = h_3 \begin{Bmatrix} \rho \\ \rho u \\ \rho v \\ \rho w \\ E_t \\ \rho\sigma_i \end{Bmatrix}, \qquad \boldsymbol{E}_I = h_3 \begin{Bmatrix} \rho u \\ \rho u^2 + \dfrac{p}{\gamma_\infty M_\infty^2} \\ \rho uv \\ \rho uw \\ (E_t + p)\,u \\ \rho\sigma_i u \end{Bmatrix}$$

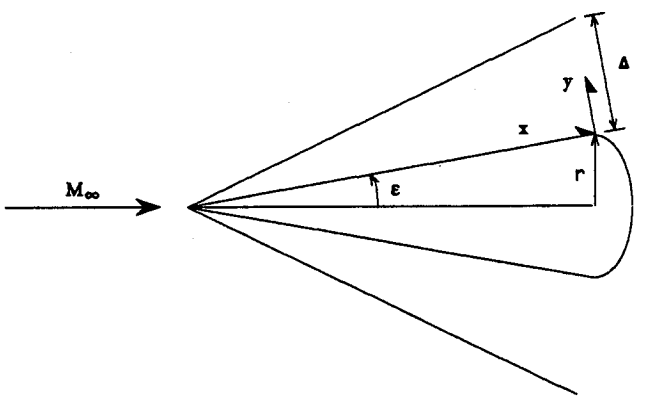

Fig. 1 Coordinate system and definition of geometry.

$$\boldsymbol{F}_I = h_3 \begin{Bmatrix} \rho v \\ \rho uv \\ \rho v^2 + \dfrac{p}{\gamma_\infty M_\infty^2} \\ \rho vw \\ (E_t + p)\,v \\ \rho\sigma_i v \end{Bmatrix}, \qquad \boldsymbol{G}_I = \begin{Bmatrix} \rho w \\ \rho uw \\ \rho vw \\ \rho w^2 + \dfrac{p}{\gamma_\infty M_\infty^2} \\ (E_t + p)\,w \\ \rho\sigma_i w \end{Bmatrix}$$

$$\boldsymbol{H}_I = \begin{Bmatrix} 0 \\ -m\left(\rho w^2 + \dfrac{p}{\gamma_\infty M_\infty^2}\right)\sin\varepsilon \\ -m\left(\rho w^2 + \dfrac{p}{\gamma_\infty M_\infty^2}\right)\cos\varepsilon \\ m\rho w\,(u\sin\varepsilon + v\cos\varepsilon) \\ 0 \\ 0 \end{Bmatrix}, \qquad \boldsymbol{R} = h_3 \begin{Bmatrix} 0 \\ 0 \\ 0 \\ 0 \\ 0 \\ R_i \end{Bmatrix}$$

$$\boldsymbol{E}_V = \frac{h_3}{Re_L} \begin{Bmatrix} 0 \\ S_{xx} \\ S_{yx} \\ S_{zx} \\ \gamma_\infty M_\infty^2 (uS_{xx} + vS_{yx} + wS_{zx}) - q_x \\ -\hat{j}_{ix} \end{Bmatrix}$$

$$\boldsymbol{F}_V = \frac{h_3}{Re_L} \begin{Bmatrix} 0 \\ S_{xy} \\ S_{yy} \\ S_{zy} \\ \gamma_\infty M_\infty^2 (uS_{xy} + vS_{yy} + wS_{zy}) - q_y \\ -\hat{j}_{iy} \end{Bmatrix}$$

$$\boldsymbol{G}_V = \frac{1}{Re_L} \begin{Bmatrix} 0 \\ S_{xz} \\ S_{yz} \\ S_{zz} \\ \gamma_\infty M_\infty^2 (uS_{xz} + vS_{yz} + wS_{zz}) - q_z \\ -\hat{j}_{iz} \end{Bmatrix}$$

$$\boldsymbol{H}_V = \frac{1}{Re_L} \begin{Bmatrix} 0 \\ -mS_{zz}\sin\varepsilon \\ -mS_{zz}\cos\varepsilon \\ m\,(S_{xz}\sin\varepsilon + S_{yz}\cos\varepsilon) \\ 0 \\ 0 \end{Bmatrix}$$

The following constitutive equations are also needed:

$$\sum_{i=1}^{nsp} \sigma_i \hat{M}_i = 1 \quad \text{(mass fractions sum to one)} \tag{6a}$$

$$p = \sum_{i=1}^{nsp} p_i \quad \text{(Dalton's law of partial pressures)} \tag{6b}$$

$$p_i = \rho \sigma_i T \quad \text{(each species is a perfect gas)} \tag{6c}$$

$$E_t = \rho h(T) - p + (1/2)\gamma_\infty M_\infty^2 \rho(u^2 + v^2 + w^2) \tag{6d}$$

$$h(T) = \sum_{i=1}^{nsp} \sigma_i \hat{h}_i(T) \tag{6e}$$

The dynamic viscosity and translational thermal conductivity are computed using the mixture laws of Brokaw,[14] as Yos[15] had done. The internal thermal conductivity is computed using the method described by Hirschfelder.[16–18] The species molar fluxes $\hat{j}_i$ are computed using the multicomponent diffusion model described by Curtiss and Hirschfelder,[19] but only diffusion due to concentration gradients is included. Diffusion due to pressure and temperature gradients and body forces is neglected.

The law of mass action is used to compute the molar rate of production R_i of each species assuming that the following elementary reactions occur in the flow:

$$M + O_2 \rightleftarrows O + O + M \tag{7a}$$

$$M + N_2 \rightleftarrows N + N + M \tag{7b}$$

$$M + NO \rightleftarrows N + O + M \tag{7c}$$

$$N_2 + O \rightleftarrows NO + N \tag{7d}$$

$$O + NO \rightleftarrows N + O_2 \tag{7e}$$

where M represents an actual collision partner (a "third body") that exchanges energy in the reaction and hence makes it possible.

The thermophysical and thermochemical data needed for the analysis have been taken from a variety of sources. See Stuckert[20] for the data and corresponding references.

III. Basic-State Analysis

The basic state is taken to be the solution of the parabolized Navier-Stokes (PNS) equations.[8,21–24] The PNS equations can be solved by marching in ξ. Here, the initial conditions are generated by assuming that the flow is approximately conical[23] near the apex of the sharp cone. The numerical method is based on the three-point backward-Euler method and the Beam-Warming algorithm.[25] To eliminate spurious numerical oscillations that may adversely affect the stability analysis, a shock-fitting scheme is also used. Hence, no artificial dissipation is required for the simple geometry investigated here because there are no discontinuities embedded in the shock layer. To suppress PNS departure solutions, the Vigneron technique is used. Finally, a stretching function clusters grid points near the edge of the boundary layer, a location where the basic state varies rapidly and that also lies in the vicinity of the critical point of the disturbance solutions at hypersonic Mach numbers; 481 grid points are used between the body and the bow shock for both the basic-state and stability analyses.

To help validate the basic-state software, the PNS solution is compared with that of Prabhu et al.[24] The geometry and flight conditions are as follows.

A. Boundary Conditions

The flowfield is created by a 10-deg half-angle sharp cone flying at 8100 m/s (Mach 25) at an altitude of 60.96 km where the ambient temperature and pressure are 252.6 K and 2.008×10^{-4} atm, respectively. For the reacting-gas cases (local chemical equilibrium and nonequilibrium), the freestream mole fractions are assumed to be those shown in Table 1.

The surface of the cone is assumed to be at a constant temperature of 1200 K. This wall temperature is a small fraction (3.7%) of the stagnation temperature and is slightly less than both the post-shock temperature and the boundary-layer edge temperature. The wall is also assumed to be noncatalytic for the nonequilibrium-air analyses, whereas for the equilibrium-air analyses the mixture is assumed to be in local chemical equilibrium at the cone's surface.

The length scale chosen for the computations is $L_{ref} = 1$ m. This reference length is simply chosen for convenience since the cone is sharp and may be arbitrarily long. The Reynolds number based on these freestream conditions and reference length is 1.399×10^5.

B. Basic-State Results

The flowfield was computed by Prabhu et al.[24] except that they assumed a different freestream gas composition. (The values we used model the composition of air between sea level and a 90-km altitude as given in the U.S. Standard Atmosphere[26]: 78.084% N_2, 20.948% O_2, 0.934% Ar, 0.0314% CO_2, 0.00182% Ne, 0.00052% He, 0.000114% Kr, 0.0002% CH_4 . . ..) They also assumed that all of the mass diffusion coefficients are the same (binary diffusion model) with a constant Lewis number equal to 1.4 for each species. The reaction rates, transport-property mixture rules, and constituent transport properties are also different. (We have used the most recent data available. Older viscosity data have been considered[27] for the last 20 years to be systematically in error at higher temperatures yet are still used by many in the field of CFD. Similarly, Ref. 24 used Wilke's mixture rules,[28] which have been shown to be inaccurate[29,30] for high-temperature ionized mixtures.) Moreover, they did not use a shock-fitting scheme and instead chose to capture the bow shock. This necessitated the use of artificial viscosity that Tannehill et al.[31] state had a significant effect on the computed mass-fraction profiles. Nevertheless, Figs. 2 and 3 (with y^* nondimensionalized by δ^*) show that the agreement between the present results and the (digitized) results of Ref. 24 is quite reasonable.

Comparisons[20] (not shown) were also made between the perfect-gas, equilibrium-air, and nonequilibrium-air PNS solutions and also the perfect-gas similarity solution. Both the perfect-gas PNS solution and the perfect-gas boundary-layer similarity solution were computed assuming a constant specific heat $c_p = 3.5$, a constant Prandtl number = 0.70, and the Sutherland viscosity law for air. The perfect-gas PNS solution and the perfect-gas similarity solution are in excellent agreement throughout the boundary layer.

IV. Linear Stability Analyses

A. Normal-Mode Solutions

The stability analysis is begun by linearizing the complete Navier-Stokes equations about the laminar shock-layer solution $\boldsymbol{Q}_b$ for the sharp cone. This yields the linear disturbance equations. Here they are formulated in terms of the variables $\boldsymbol{Q}_d = y_\eta \boldsymbol{U} = y_\eta h_3(\rho, \rho u, \rho v, \rho w, E_t, \rho\sigma_i)^T$ in the basic-state shock-fitted coordinate system. The multiplicative factor $y_\eta h_3$ in the definition of $\boldsymbol{Q}_d$ is the Jacobian of the coordinate transformation from Cartesian coordinates to the shock-fitted coordinates.

Approximating the linear disturbance equations as being separable partial differential equations (the boundary conditions must also be separable) in τ, ξ, and ζ (parallel-flow approximation), they admit normal-mode solutions:

$$\boldsymbol{Q}_d = \boldsymbol{Q}_a(\eta)\exp(-i\omega\tau + i\alpha\xi + i\beta\zeta) + \text{c.c.} \tag{8}$$

where c.c. denotes the complex conjugate, and $\boldsymbol{Q}_a$ is the complex-valued amplitude function; $\omega/2\pi$ is the complex-valued frequency, α is the complex-valued wave number in the ξ direction, and β (for

Table 1 Freestream mole fractions for reacting-gas cases

Species	O_2	O	NO	N	N_2
Mole fraction	0.21	0	0	0	0.79

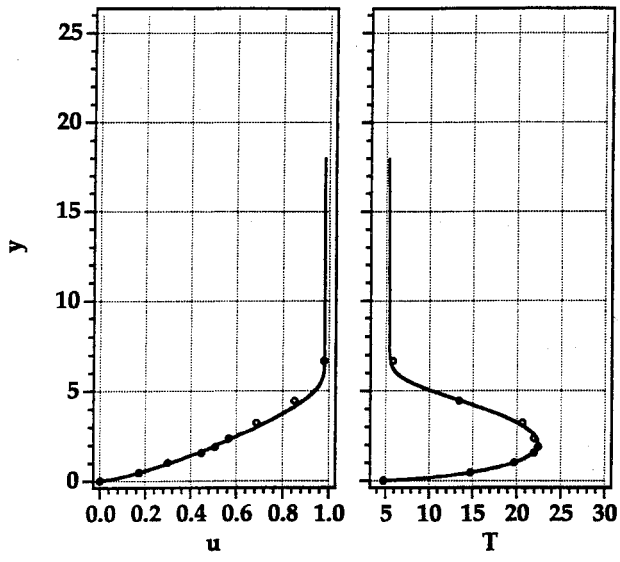

Fig. 2 Comparison with Prabhu et al.[24] (symbols) of computed (lines) velocity and temperature profiles for air in chemical nonequilibrium, $x^* = 3.5$ m.

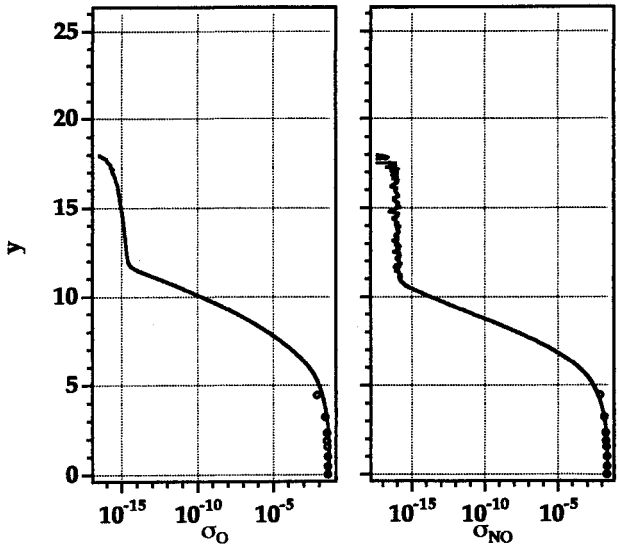

Fig. 3 Comparison with Prabhu et al.[24] (symbols) of computed (lines) atomic-oxygen and nitric-oxide concentration: mixture density ratios for air in chemical nonequilibrium, $x^* = 3.5$ m.

two-dimensional or axisymmetric basic states) is the real-valued wave number in the spanwise (two-dimensional) or circumferential (axisymmetric) direction.

The selection of $\boldsymbol{Q}_d$ as the disturbance variables helps validate the approximation that the normal modes are solutions by eliminating many terms in the disturbance equations that would otherwise make the equations nonseparable. The factor h_3 in the definition of $\boldsymbol{Q}_d$ accounts for virtually all effects of the transverse curvature of the cone.[20,32] The factor y_η also affects the streamwise growth of $\boldsymbol{Q}_d$ because of the increasing shock-layer thickness. Both variations of the Jacobian must be accounted for when computing the spatial growth rate of $(\rho, \rho u, \rho v, \rho w, E_t, \rho\sigma_i)^T$ from the following cone boundary-layer stability results.

The coordinates used for the stability analysis also influence the approximation that the disturbance equations are separable. This is because the Navier-Stokes equations are nonlinear and so the linearized equations depend upon the variations of the laminar-flow solution. Most of the nonseparable terms that are neglected involve the derivatives of $(\rho, \rho u, \rho v, \rho w, E_t, \rho\sigma_i)^T$ with respect to ξ. However, since we use the basic-state shock-fitted coordinates, this approximation is exact in the inviscid limit for then the basic state is conical. The normal velocity component is not zero in a conical flow, though, and so is not neglected as it usually is.

B. Boundary Conditions

The basic-state shock-fitted coordinate system also makes it easier to apply the linearized shock-jump conditions as the disturbance boundary conditions. Although Cowley and Hall,[33] among others, have applied similar boundary conditions, no one has yet used a shock-fitted coordinate system for the stability analysis. These linearized shock-jump conditions[20] allow for a disturbance in the oblique shock and its slope but are applied at the basic-state shock location instead of the disturbed shock location.

At the surface of the cone, the velocity and temperature disturbances are zero. For the nonequilibrium calculations, the species mass fluxes are set to zero (noncatalytic wall), whereas for the equilibrium calculations the disturbances are assumed to be in chemical equilibrium.

C. Eigenanalysis

Substituting the normal-mode form for the disturbances into the linear disturbance equations yields a system of homogeneous ordinary differential equations depending upon the three wave parameters α, β, and ω. These homogeneous equations, together with the homogeneous boundary conditions, represent an eigenvalue problem for the eigenvector $\boldsymbol{Q}_a$.

For temporally evolving disturbances, α is taken to be real valued, and ω is determined as a complex eigenvalue of the linear disturbance equations. This is a linear eigenvalue problem because only first derivatives of time appear in the linear disturbance equations.

For spatially evolving flows, ω is taken to be real valued, and α is determined as a complex eigenvalue of the linear disturbance equations. In this case, the eigenvalue problem is nonlinear because the viscous terms in the disturbance equations depend upon second derivatives with respect to ξ.

The results presented here are from a spatial analysis. To obtain them, the disturbance equations were discretized with second-order-accurate finite differences. All of the temporal eigenvalues of the resulting algebraic system were then found using the QR algorithm (e.g., Ref. 34). Generalized inverse Rayleigh iteration[35,36] and the Newton-Raphson method were then used to compute the eigenvectors and corresponding spatial eigenvalues for the unstable disturbances.

D. Testing

Some of the testing we have done to validate our calculations has involved comparisons with flat-plate perfect-gas boundary-layer stability analyses available in the literature.[37] Plotting accuracy of the spatial growth rate is typically obtained using 80–100 grid points. We have also completed some reacting-flow stability analyses at low supersonic Mach numbers to verify that the perfect-gas results are obtained for flows in which the chemical reactions are unimportant.

Another test involved a comparison with Malik's[5] perfect-gas and equilibrium-air stability analyses of a Mach 10 adiabatic flat-plate boundary layer. Our results (assuming normal modes for $\boldsymbol{U}$, not $\boldsymbol{Q}$; making the parallel-flow approximation; and imposing homogeneous boundary conditions at the shock) are compared with Malik's in Fig. 4.

The top panel of Fig. 4 compares our computed spatial growth rate with Malik's, assuming air to be thermally and calorically ($\gamma = 1.4$) perfect. We used both the Blasius solution (solid line) and the PNS solution (dashed line) for the boundary layer. Malik (symbols) does not state how he computed the boundary layer, but we

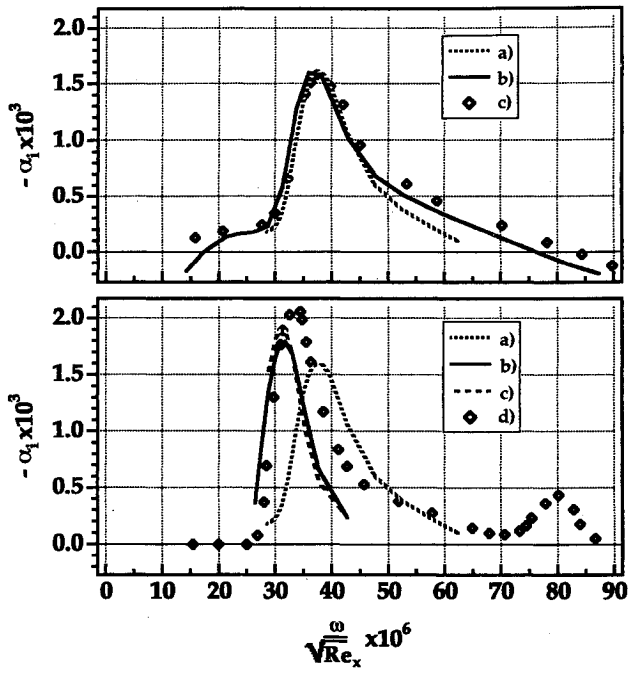

Fig. 4 Spatial growth rates of disturbances in a Mach 10 adiabatic flat-plate boundary-layer flow of a perfect gas (top panel) and reacting gas (bottom panel). Top panel: a) PNS basic state, b) similarity solution, and c) Malik's[5] results. Bottom panel: a) perfect-gas PNS, b) PNS nonequilibrium, c) PNS equilibrium, and d) Malik[5] (equilibrium).

presume he used the Blasius solution. The PNS solution was obtained using 121 points in the wall-normal direction between the plate and the shock induced by the displacement effects of the boundary layer. As can be seen, all of the results are in very good agreement. In addition to validating our stability code, these results also demonstrate the suitability of our PNS solutions for stability analyses.

The lower panel in Fig. 4 compares our computed spatial growth rates with Malik's equilibrium-air results. All of our results shown use the PNS solution, either for a perfect gas (long dashed line), equilibrium air (short dashed line), or nonequilibrium air (solid line). Here our equilibrium- and nonequilibrium-air solutions agree very well, indicating that the approximation of local chemical equilibrium is a reasonable one. Our results also agree fairly well with Malik's[5] (symbols) but indicate that the most unstable disturbance has a slightly smaller growth rate and occurs at a lower frequency. Malik[5] does not state how he computed the equilibrium-air boundary layer, or what transport properties and thermodynamic data he used, and so it is difficult for us to comment on these differences. In any case, as seen in Fig. 4, the most unstable disturbance is shifted to a lower frequency in the equilibrium and nonequilibrium flows relative to the higher frequency in the perfect-gas case. This was noted by Malik[5] and is confirmed here. An explanation for this shift is offered later.

E. Results

Here we present our stability analyses of the laminar shock layer on the Mach 25, 10-deg sharp cone for three different approximations of the thermochemistry: perfect gas, equilibrium air, and nonequilibrium air. Since the inclusion of the nonequilibrium chemistry is what makes this work unique, most of the results presented here are for the nonequilibrium shock layer. Data at one station on the cone, $\sqrt{Re_x} = 1022.3$, are presented. Complete results for all of the different cases at different frequencies, spanwise wave numbers, and stations can be found in Ref. 20.

As Mack[2,3] has shown for a perfect gas, there are multiple families of unstable modes. Here, a family is defined as the locus of eigenvalues α traced out as the parameters ω and β are varied. The panels of Fig. 5 show the different spatial growth rates $-\alpha_i$ for three different unstable families of perfect-gas (short dashed line), equilibrium-air (solid line) and nonequilibrium-air (long dashed line) solutions as functions of ω for five different values of β: 0 (top row), 10, 20, 30, and 40 (bottom row). The left column shows the first family, the middle column the second family, and the right column the third family.

Figures 6–9 show some of the $\beta = 0$ eigenvectors, normalized by the value of the disturbance density at the surface of the cone. The bow shock is located at the largest plotted value of y. (Here, y^* has been nondimensionalized by δ^*.)

The first family of disturbances (Fig. 5) with frequency $0 < \omega/\sqrt{Re_x} \times 10^6 < 150$ (approximately) has features characteristic of Mack's first mode and correspond to the Tollmien-Schlichting waves in an incompressible boundary layer.[2,3] As Mack[2,3] and oth-

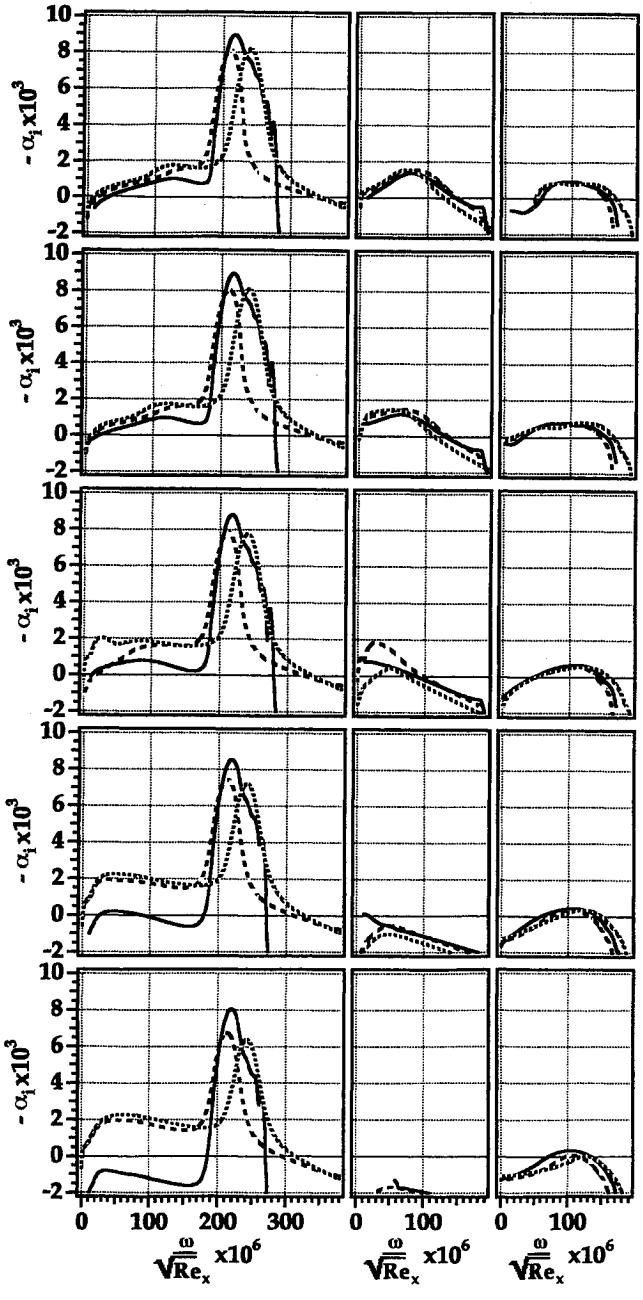

Fig. 5 Spatial growth rates of disturbances in the Mach 25, 10-deg half-angle sharp-cone shock layer. Solid line: equilibrium air. Long-dash line: nonequilibrium air. Short-dash line: perfect gas. Left column of panels for first family, middle column for second family, and right column for third family. Different rows of panels correspond to different azimuthal wave numbers: first row, $\beta = 0$; second row, $\beta = 10$; third row, $\beta = 20$; fourth row, $\beta = 30$; and fifth row, $\beta = 40$.

ers have shown, these modes for compressible flow are most unstable when they are oblique (β nonzero). Our results (Fig. 5) are consistent with this. Figure 5 also shows that, whereas the perfect-air and nonequilibrium-air results are comparable for all spanwise wave numbers, the first modes of the first family of equilibrium-air solutions are much more stable than both the perfect-gas and nonequilibrium-air solutions at the higher spanwise wave numbers. For these modes, the approximation of local chemical equilibrium is clearly not good.

An eigenvector corresponding to one of the first-mode nonequilibrium-air solutions is shown in Figs. 6 and 7. It corresponds to the solution at the lowest-frequency ($\omega/\sqrt{Re_x} \times 10^6 = 151$) local maximum in the growth rate of the first family shown in Fig. 5. The low-pressure phase change (much less than 180 deg, see Fig. 6) across the boundary layer identifies the mode as a first mode. This mode is outgoing because the phase of the disturbance pressure decreases with y in the inviscid region of the shock layer. Its phase speed is $0.91U_\infty$. Alternatively, since the edge velocity is $0.98U_\infty$, its phase speed is $0.93U_e$. Since the edge Mach number is 10.6, the mode is subsonic relative to the boundary-layer edge velocity. The critical point where the phase speed of the mode equals the flow velocity is at $y = 4.6$. Note the zero in the magnitude and 180-deg phase shift in the disturbance of the wall-normal mass flux at the critical point (Fig. 6). Also note that the phase in the wall-normal disturbance mass flux is 90 deg and is virtually constant between the wall and the critical point.

The wall-normal mass-flux phase of 90 deg at the wall is to be expected from the equation of conservation of mixture mass evaluated at the surface: $-i\omega\rho + \partial(\rho v)/\partial y = 0$. Since the eigenvector has been normalized such that $\rho = 1$ at the surface, and since $\omega_r >> \omega_i$, the phase of $\partial(\rho v)/\partial y$ is almost 90 deg different than the phase of ρ at the surface. Since the derivative of the phase at the surface is virtually zero (Fig. 6), the phase of $\partial(\rho v)/\partial y$ = the phase of $\rho v = 90$ deg at the surface.

Figure 7 shows the disturbances in the molecular and atomic-oxygen concentrations for the first mode of the first family of nonequilibrium-air solutions. Note that the magnitude of the disturbance in the atomic-oxygen concentration is zero outside of the concentration boundary layer where the mean-flow atomic-oxygen concentration is zero. (The disturbance phase is arbitrary when the magnitude is zero and so is simply set to a constant between the edge of the concentration boundary layer and the bow shock.) This is to be expected because the concentration must be a positive definite quantity; it cannot oscillate with a nonzero magnitude about a zero basic-state value. Similarly, the disturbances in the concentrations of NO and N (not shown) are also zero in the inviscid region of the shock layer. These features are present in all of the nonequilibrium- and equilibrium-air eigenvectors, and their consistency with the rest of the analysis helps to validate our results.

At frequencies in the range $150 < \omega/\sqrt{Re_x} \times 10^6 < 400$, the first family (left column) of solutions shown in Fig. 5 are characteristic of Mack's second mode. These second-mode disturbances are most unstable when they are axisymmetric (or two dimensional[2,3]).

Figure 8 shows the nonequilibrium-air eigenvector for the most amplified first-family second-mode axisymmetric solution ($\omega/\sqrt{Re_x} \times 10^6 = 209$). The pressure phase change (127 deg) across the boundary layer is what identifies it as Mack's second mode. It is a subsonic, outgoing mode with phase speed $0.91U_\infty$ or $0.93U_e$. The critical point is at $y = 4.6$. Although the magnitude of the wall-normal mass-flux disturbance is no longer zero at the critical point, it exhibits a local minimum there. Also, the disturbance ρv changes phase across the critical layer by 100 deg. As with all of the modes, the disturbance ρv phase at the wall = −270 deg (90 deg modulo 360 deg). However, in contrast to the longer-wavelength first-mode disturbances of all three families, the magnitude of the second-mode disturbance pressure behind the shock is virtually zero (0.5% of maximum). Similarly, the disturbance ρv behind the shock is also much smaller (1.9% of maximum).

Although the maximum amplification rate of the first-family second mode is comparable for perfect gas, equilibrium air, and nonequilibrium air, the frequency at which the maximum occurs in

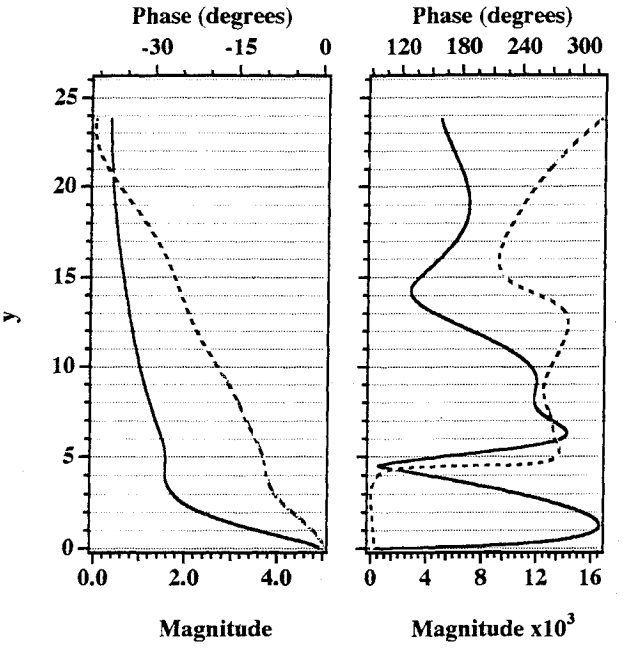

Fig. 6 Magnitude (solid line) and phase (dashed line) of disturbance pressure (left) and wall-normal mass flux (right). First family of nonequilibrium-air solutions; α = (0.169, −0.00164), β = 0, ω = 0.154, and $\sqrt{Re_x}$ = 1022.3.

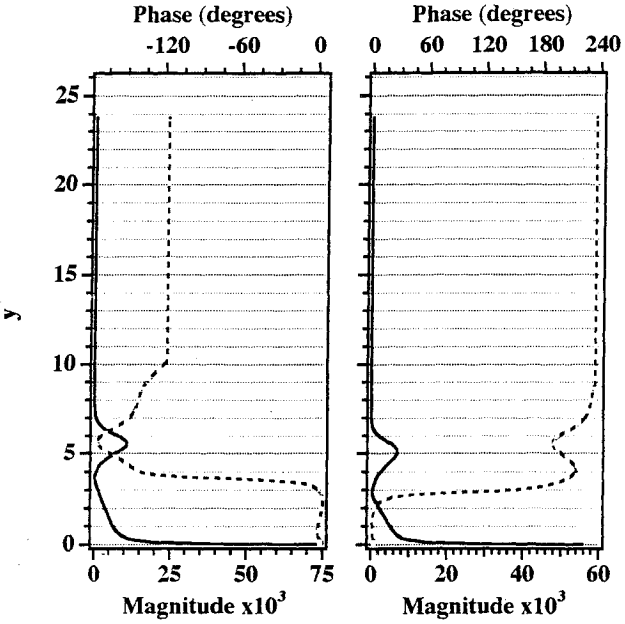

Fig. 7 Magnitude (solid line) and phase (dashed line) of disturbances in atomic-oxygen concentration; mixture density ratio (left), and nitric-oxide concentration; mixture density ratio (right). First family of nonequilibrium-air solutions; α = (0.169, −0.00164), β = 0, ω = 0.154, and $\sqrt{Re_x}$ = 1022.3.

the reacting-gas cases is lower than in the perfect-gas case. This is also evident in the results[5] for the second- and third-mode[5] solutions for the Mach 10 adiabatic flat-plate boundary layer (Fig. 4).

The second mode likely shifts to lower frequencies because the region of relative supersonic flow [the region of flow within the boundary layer where either the flow is traveling supersonically relative to the disturbance or the disturbance is traveling supersonically relative to the flow (i.e., typically at the body surface within the cooler, denser, reacting-gas boundary layers is larger due to the lower local sound speed. This is clear if one considers Mack's[2] ap-

proximate expression for the neutral wave numbers of an inviscid disturbance in a parallel perfect-gas boundary layer:

$$\alpha_{s(n+1)} - \alpha_{s(n)} = \frac{\pi}{\int_0^{y_1} \sqrt{\bar{M}^2 - 1}\, dy} \tag{9}$$

where y_1 is the location of the relative sonic point and $\bar{M}^2$ is the square of the relative Mach number of the flow. (A related expression obtained by Mack estimates the magnitudes of the neutral eigenvalues themselves. Mack[2] states, however, that it is not very accurate for this purpose even though it leads to the expression just given, which is accurate in many circumstances.) The integral appearing in the denominator has been evaluated using the phase speeds equal to the velocity at the generalized inflection points of the corresponding shock layers (i.e., perfect gas, equilibrium air, and nonequilibrium air). The results are shown in Table 2. Although the perfect-gas and nonequilibrium-air mean flows have very similar generalized inflection profiles[20] and the generalized inflection points occur at almost the same locations, the value of the integral appearing in the preceding equation is much larger in the nonequilibrium-air case. In the equilibrium-air case, there are not any generalized inflection points within the boundary layer. There does appear to be one within the inviscid region of the shock layer although it is difficult to resolve numerically because of the very small gradients there relative to those in the boundary layer. In any case, one should remember that the preceding simple expression is for perfect-gas flows only and does not in any way take into account the effects of chemical reactions.

In addition to the fact that the second mode of the first family of equilibrium-air solutions occurs at a lower frequency, the growth rate curve for the first family of equilibrium-air solutions also has multiple local maxima in the frequency range $200 < \omega/\sqrt{Re_x} \times 10^6 < 300$ that are not present in the perfect-gas or nonequilibrium-air results. The equilibrium-air modes at the local maxima have phase speeds supersonic relative to the boundary-layer edge velocity, whereas in the perfect-gas and nonequilibrium-air flows these modes are relatively subsonic at the same frequencies.

Figure 9 shows an equilibrium-air solution at one of these local maxima. Again, this solution has phase speed supersonic relative to the boundary-layer edge velocity. The phase of the disturbance

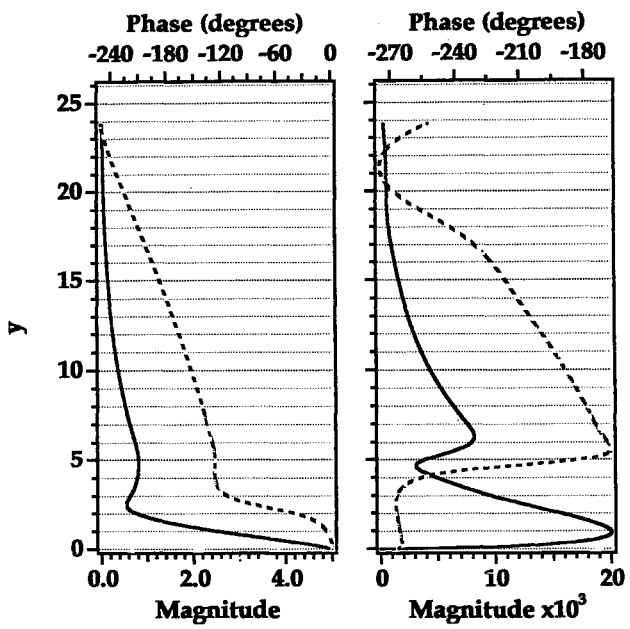

Fig. 8 Magnitude (solid line) and phase (dashed line) of disturbance pressure (left) and wall-normal mass flux (right). First family of nonequilibrium-air solutions; α = (0.235, −0.00812), β = 0, ω = 0.124, and $\sqrt{Re_x}$ = 1022.3.

Table 2 Location of generalized inflection points and value of wave number spacing integral for different models of the flow

Model	y at generalized inflection point	$\int_0^{y_1} \sqrt{\bar{M}^2 - 1}\, dy$
PNS perfect gas	2.96844	4.02162
Perfect-gas similarity solution	3.03166	4.14553
PNS nonequilibrium air	3.03101	4.86724
PNS equilibrium air	——	——
PNS perfect gas	4.39413	7.42266
Perfect-gas similarity solution	4.29631	7.16719
PNS nonequilibrium air	4.20865	8.2549
PNS equilibrium air	——	——
PNS perfect gas	17.0357	9.69725
Perfect-gas similarity solution	N/A	N/A
PNS nonequilibrium air	16.6718	11.3631
PNS equilibrium air	13.2963	11.1159

pressure in the inviscid region of the shock layer also indicates that this solution is still outgoing. However, because it is supersonic, it interacts very strongly with the shock.

Figure 9 also shows that the magnitudes of the disturbance pressure and wall-normal mass flux are oscillatory in y in the inviscid region of the shock layer. Such oscillatory solutions (at least neutral ones) can be expected for inviscid disturbances traveling supersonically relative to the inviscid region of the shock layer on a flat plate. Consider for a perfect gas the equation governing the amplitude function p_a for the disturbance pressure[2,3]:

$$p_a'' - [\log(\bar{M}^2)]' \cdot p_a' - \alpha^2(1 - \bar{M}^2)\, p_a = 0 \tag{10}$$

where $'$ denotes differentiation with respect to y and $\bar{M}$ is the Mach number of the disturbance phase speed relative to the mean flow:

$$\bar{M} = \frac{(u - c)}{\sqrt{T}} M_e \tag{11}$$

Here $c = \omega/\alpha$, M_e is the Mach number at the boundary-layer edge, and the temperature and all velocities have been nondimensionalized by the boundary-layer edge temperature and speed, respectively.

In the inviscid region of the shock layer, $u \approx 1$ and $T \approx 1$. In this region of the flow, Eq. (10) becomes

$$p_a'' - \alpha^2(1 - \bar{M}^2) \cdot p_a = 0 \tag{12}$$

which has solutions of the form

$$p_a = a_1\varphi_1 + a_2\varphi_2 \tag{13}$$

where a_1 and a_2 are real numbers and

$$\varphi_1 = \exp\left\{-\frac{1}{2}\left[\sqrt{|\alpha^2(1 - \bar{M}^2)|}\right](\sin\phi)\, y\right\} \times \exp\left\{\frac{i}{2}\left[\sqrt{|\alpha^2(1 - \bar{M}^2)|}\right](\cos\phi)\, y + i\theta_1\right\} \tag{14a}$$

$$\varphi_2 = \exp\left\{\frac{1}{2}\left[\sqrt{|\alpha^2(1 - \bar{M}^2)|}\right](\sin\phi)\, y\right\} \times \exp\left\{-\frac{i}{2}\left[\sqrt{|\alpha^2(1 - \bar{M}^2)|}\right](\cos\phi)\, y + i\theta_2\right\} \tag{14b}$$

Also, $|\alpha^2(1-\bar{M}^2)|$ is the magnitude and ϕ is the phase of the complex number $\alpha^2(1-\bar{M}^2)$; θ_1 and θ_2 are real numbers, and $i = \sqrt{-1}$.

One of the two solutions φ_1 and φ_2 grows, whereas the other decays exponentially with respect to y. Classical boundary-layer stability theory takes $0 \le y < \infty$. In this case, the solution (13) will only be bounded as $y \to \infty$ if the coefficient, either a_1 or a_2, of the exponentially growing solution is zero. Which of the solutions φ_1 and φ_2 grows and which decays exponentially depends on the sign of $\sin\phi$.

Since ϕ is the phase of the complex number $\alpha^2(1-\bar{M}^2)$, $\sin\phi$ will have the same sign as the imaginary part of $\alpha^2(1-\bar{M}^2)$:

$$\alpha^2(1-\bar{M}^2) = \frac{\alpha^2u^2-\omega^2}{T}M_e^2-\alpha^2 \tag{15a}$$

$$= \frac{(\alpha_r^2-\alpha_i^2)u^2-\omega^2}{T}M_e^2-(\alpha_r^2-\alpha_i^2)$$

$$+2i\alpha_r\alpha_i\left(\frac{u^2}{T}M_e^2-1\right) \tag{15b}$$

The sign of $\sin\phi$ is thus the same as the sign of $\alpha_r\alpha_i[(u^2/T)M_e^2 - 1]$. Outside of the boundary layer, $u \approx 1$ and $T \approx 1$, and so $\text{sign}(\sin\phi) = \text{sign}[\alpha_r\alpha_i(M_e^2-1)]$. For supersonic boundary layers, $M_e > 1$, and so $\text{sign}(\sin\phi) = \text{sign}(\alpha_r\alpha_i)$. Finally, since α_r is almost always greater than zero, $\text{sign}(\sin\phi) = \text{sign}(\alpha_i)$. Hence, as shown by Mack,[2] in classical boundary-layer stability theory, only amplified outgoing disturbances ($a_1 = 0$) and damped incoming ones ($a_2 = 0$) satisfy the boundary conditions in the limit $y \to \infty$.

In the bounded domain $0 \le y \le \Delta_b$, however, both solutions φ_1 and φ_2 are admissible. That a solution with nonzero a_1 and a_2 exhibits oscillations with y in its magnitude can be seen by computing the square of the magnitude:

$$|p_d|^2 = a_1^2\exp\left\{-\left[\sqrt{|\alpha^2(1-\bar{M}^2)|}\right](\sin\phi)\,y\right\}$$

$$+a_2^2\exp\left\{-\left[\sqrt{|\alpha^2(1-\bar{M}^2)|}\right](\sin\phi)\,y\right\}$$

$$+2a_1a_2\cos\left\{\left[\sqrt{|\alpha^2(1-\bar{M}^2)|}\right](\cos\phi)\,y+\theta_1-\theta_2\right\} \tag{16}$$

If either a_1 or a_2 is zero, then the magnitude will decay exponentially with y; otherwise, it will oscillate with y. The wavelength of the magnitude of the oscillations in y for the mode shown in Fig. 9 calculated from Eq. (16) is approximately 2.7. However, the actual wavelength shown in the figure appears to be slightly longer. The analysis presented here is for a parallel flow of an inviscid perfect gas, though, whereas the computed solution is for a viscous, equilibrium-air flow over a cone.

In conclusion, the oscillation with y of the disturbance pressure magnitude is evidence that the eigenvector shown in Fig. 9 is the sum of an incoming and an outgoing disturbance. These oscillations occur only because the shock-layer thickness is finite. This eigenvector is not one of Mack's "conventional" higher modes because the phase change of the disturbance pressure across the boundary layer remains about −150 deg. In this region, the disturbance still exhibits second-mode behavior.

Returning to Fig. 5, one can see that, although the character of the first family of solutions depends significantly on the proper modeling of the chemical reactions, the growth rates of the second and third families of perfect-air, equilibrium-air, and nonequilibrium-air solutions are all very similar. Both the second and third families have phase speeds subsonic relative to the boundary-layer edge velocity, but the third-family phase speeds are greater than

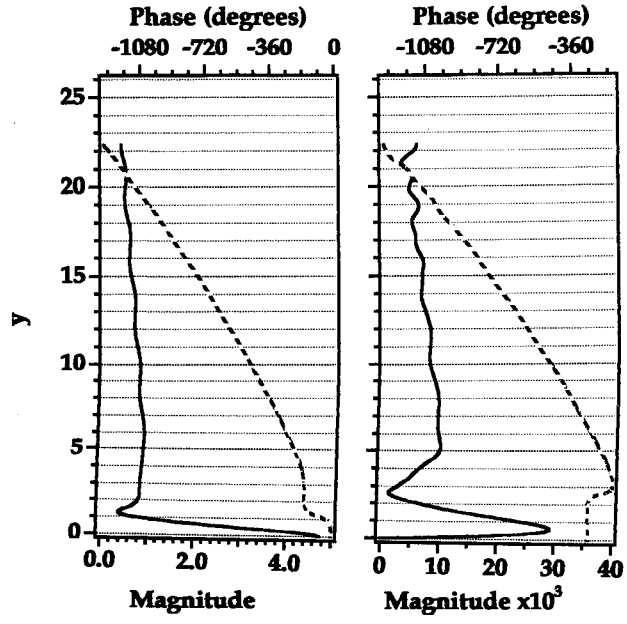

Fig. 9 Magnitude (solid line) and phase (dashed line) of disturbance pressure (left) and wall-normal mass flux (right). First family of nonequilibrium-air solutions; α = (0.364, −0.00415), β = 0, ω = 0.279, and $\sqrt{Re_x}$ = 1022.3.

the edge velocity whereas the second-family phase speeds are less than the edge velocity. The third family thus consists of Mack's[2,3] regular solutions for which there is no critical layer where the phase speed and mean-flow velocity are equal. Finally, the lowest-frequency disturbances ($\omega/\sqrt{Re_x} \times 10^6 < 50$) in these families are most unstable when they are oblique, but the higher-frequency modes are most unstable when they are axisymmetric. Eigenvectors for the second and third families are shown in Stuckert.[20] They clearly show that the first mode disturbances are not zero at the bow shock.

V. Conclusions

It is clear that the equilibrium and nonequilibrium solutions can differ significantly depending on the rates of the reactions relative to the time scales of convection and diffusion. In particular, the equilibrium solutions shown here exhibited supersonic modes, each of which is a superposition of incoming and outgoing amplified solutions in the inviscid region of the shock layer. No similar solutions were found for the nonequilibrium shock layer. The magnitudes of these modes oscillate with y in the inviscid region of the shock layer. This behavior is possible only because the shock layer has a finite thickness. They are also unlike Mack's higher modes (except for the second) in that the disturbance-pressure phase for all of these supersonic modes changes most across the inviscid region of the shock layer. [The disturbance-pressure phase change for Mack's higher modes occurs across the viscous region of the flow (i.e., the boundary layer).] In fact, the disturbance-pressure phase change for all of these supersonic modes through the boundary layer is comparable to that of Mack's second mode.

Another effect of the chemical reactions is to increase the size of the region of relative supersonic flow primarily by reducing the temperature in the boundary layer through endothermic reactions, increasing the density, and hence increasing the speed of sound and local relative Mach numbers. This reduces the frequency of the higher modes; in particular, the most unstable one—the second mode. The higher modes in the reacting-gas cases are also more unstable relative to the corresponding perfect-gas modes. The first modes are, however, more stable.

Finally, the finite thickness of the shock layer has a significant effect on the first-mode solutions of all of the families. The effect on higher-mode, higher-frequency solutions does not seem to be as large as long as they are subsonic. This is perhaps what one would

intuitively expect because the shock is likely "stiff" and hence difficult to perturb with smaller wavelength, larger wave number, higher frequency disturbances. However, the nonparallel effects are known to be large for first-mode solutions, and so a complete quantitative description of the effects of the finite shock-layer thickness awaits either a parabolized stability equations solution or a direct Navier-Stokes analysis.

Acknowledgments

This work was supported by the Air Force Office of Scientific Research, the National Science Foundation under the Presidential Young Investigator Award, General Dynamics/Fort Worth, and McDonnell Douglas/St. Louis.

References

[1]Lees, L., and Lin, C. C., "Investigation of the Stability of the Laminar Boundary Layer in a Compressible Fluid," NACA TN 1115, 1946.

[2]Mack, L. M., "Boundary Layer Stability Theory," Jet Propulsion Lab., California Inst. of Technology, Document 900-277 (Rev. A), Pasadena, CA, Nov. 1969.

[3]Mack, L. M., "Review of Linear Compressible Stability Theory," *Stability of Time Dependent and Spatially Varying Flows*," edited by D. L. Dwoyer and M. Y. Hussaini, Springer-Verlag, New York, 1987, pp. 164–187.

[4]Malik, M. R., "Prediction and Control of Transition in Hypersonic Boundary Layers," AIAA Paper 87-1414, June 1987.

[5]Malik, M. R., "Transition in Hypersonic Boundary Layers," Fourth Symposium on Numerical and Physical Aspects of Aerodynamic Flows, Long Beach, CA, Jan. 1989.

[6]Menon, S., Anderson, J. D., and Pai, S. I., "Stability of a Laminar Premixed Supersonic Free Shear Layer with Chemical Reactions," *International Journal of Engineering Sciences*, Vol. 22, No. 4, 1984, pp. 361–374.

[7]Grinstein, F. F., and Kailasanath, K., "Effects of Chemical Energy Release on the Dynamics of Transitional Free Shear Flows," AIAA Paper 90-1452, June 1990.

[8]Anderson, D. A., Tannehill, J. C., and Pletcher, R. H., *Computational Fluid Mechanics and Heat Transfer*, McGraw-Hill, New York, 1984.

[9]Bird, R. B., Stewart, W. E., and Lightfoot, E. N., *Transport Phenomena*, Wiley, New York, 1960.

[10]Gardiner W. C., Jr., "Introduction to Combustion Modeling," *Combustion Chemistry*, edited by W. C. Gardiner, Springer-Verlag, New York, 1984, Chap. 1.

[11]Vincenti, W. G., and Kruger, C. H., Jr., *Introduction to Physical Gas Dynamics*, Krieger Publishing Co., Malabar, FL, 1965.

[12]Viviand, H. "Conservative Forms of Gas Dynamic Equations," *La Récherche Aerospatiale*, No. 1, 1974, pp. 65–68.

[13]Vinokur, M., "Conservation Equations of Gas-Dynamics in Curvilinear Coordinate Systems," *The Journal of Computational Physics*, Vol. 14, 1974, pp. 105–125.

[14]Brokaw, R. S., "Approximate Formulas for the Viscosity and Thermal Conductivity of Gas Mixtures," *The Journal of Chemical Physics*, Vol. 29, No. 2, 1958, pp. 391–397.

[15]Yos, J. M., "Transport Properties of Nitrogen, Hydrogen, Oxygen, and Air to 30,000 K," Avco Corp., TM RAD-TM-63-7, Wilmington, MA, March 1963.

[16]Hirschfelder, J. O., "Heat Transfer in Chemically Reacting Mixtures. I," *The Journal of Chemical Physics*, Vol. 26, No. 2, 1957, pp. 274–281.

[17]Hirschfelder, J. O., "Heat Conductivity in Polyatomic or Electronically Excited Gases. II," *The Journal of Chemical Physics*, Vol. 26, No. 2, 1957, pp. 282–285.

[18]Hirschfelder, J. O., "Heat Conductivity in Polyatomic, Electronically Excited, or Chemically Reacting Mixtures. III," *Sixth Symposium (International) on Combustion*, Reinhold, New York, 1957, pp. 351–366.

[19]Curtiss, C. F., and Hirschfelder, J. O., "Transport Properties of Multicomponent Gas Mixtures," *The Journal of Chemical Physics*, Vol. 17, No. 6, 1949, pp. 550–555.

[20]Stuckert, G. K., "Linear Stability Theory of Hypersonic, Chemically Reacting Viscous Flows," Ph.D. Dissertation, Dept. of Mechanical and Aerospace Engineering, Arizona State Univ., Tempe, AZ, 1991.

[21]Rudman, S., and Rubin, S. G., "Hypersonic Viscous Flow over Slender Bodies with Sharp Leading Edges," *AIAA Journal*, Vol. 6, No. 10, 1968, pp. 1883–1889.

[22]Rubin, S. G., Lin, T. C., Pierucci, M., and Rudman, S., "Hypersonic Interactions Near Sharp Leading Edges," *AIAA Journal*, Vol. 7, No. 9, 1969, pp. 1744–1751.

[23]Schiff, L. B., and Steger, J. L., "Numerical Simulation of Steady Supersonic Flow," *AIAA Journal*, Vol. 18, No. 12, 1980, pp. 1421–1430.

[24]Prabhu, D. K., Tannehill, J. C., and Marvin, J. G., "A New PNS Code for Chemical Nonequilibrium Flows," *AIAA Journal*, Vol. 26, No. 7, 1988, pp. 808–815.

[25]Beam, R. M., and Warming, R. F., "An Implicit Factored Scheme for the Compressible Navier-Stokes Equations," *AIAA Journal*, Vol. 16, No. 4, 1978, pp. 393–402.

[26]Anon., *U.S. Standard Atmosphere*, Government Printing Office, Washington, DC, 1976.

[27]Maitland, G. C., and Smith, E. B., "Critical Assessment of Viscosities of 11 Common Gases," *Journal of Chemical and Engineering Data*, Vol. 17, No. 2, 1972, pp. 150–156.

[28]Wilke, C. R., "A Viscosity Equation for Gas Mixtures," *Journal of Chemical Physics*, Vol. 18, No. 4, 1950, p. 517.

[29]Armaly, B. F., and Sutton, K., "Viscosity of Multicomponent Partially Ionized Gas Mixtures Associated with Jovian Engry," AIAA Paper 80-1495, July 1980.

[30]Armaly, B. F., and Sutton, K., "Thermal Conductivity of Partially Ionized Gas Mixtures," AIAA Paper 81-1174, June 1981.

[31]Tannehill, J. C., Levalts, J. O., Prabhu, D. K., and Lawrence, S. L., "An Upwind Parabolized Navier-Stokes Code for Chemically Reacting Flows," AIAA Paper 88-2614, June 1988.

[32]Stuckert, G. K., and Reed, H. L., "Linear Stability of Supersonic Cone Boundary Layers," *AIAA Journal*, Vol. 30, No. 10, 1992, pp. 2402–2410.

[33]Cowley, S., and Hall, P., "On the Instability of Hypersonic Flow Past a Wedge," *Journal of Fluid Mechanics*, Vol. 214, May 1990, pp. 17–42.

[34]Golub, G. H., and Van Loan, C. F., *Matrix Computations*, Johns Hopkins Univ. Press, Baltimore, MD, 1985.

[35]Wilkinson, J. H., *The Algebraic Eigenvalue Problem*, Oxford Univ. Press, New York, 1965, Chap. 9, Secs. 61 and 62.

[36]Malik, M. R., and Orszag, S. A., "Efficient Computation of the Stability of Three-Dimensional Compressible Boundary Layers," AIAA Paper 81-1277, 1981.

[37]Malik, M. R., "Numerical Methods for Hypersonic Boundary Layer Stability," *Journal of Computational Physics*, Vol. 86, 1990, pp. 376–413.